Gain-controlled taming of recurrent modulation instability

Guillaume Vanderhaegen,[1] Pascal Szriftgiser,[1] Alexandre Kudlinski,[1] Andrea Armaroli,[1,2,*] Matteo Conforti,[1] Arnaud Mussot,[1,†] and Stefano Trillo[2]

[1]*Univ. Lille, CNRS, UMR 8523-PhLAM-Physique des Lasers Atomes et Molécules, F-59000 Lille, France*

[2]*Department of Engineering, University of Ferrara, 44122 Ferrara, Italy*

(Received 28 March 2024; accepted 5 August 2024; published 25 September 2024)

We show how the recurrence phenomenon characteristic of the nonlinear stage of induced modulational instability in a passive fiber is affected by forcing. An additional linear amplification, even if extremely weak, induces separatrix crossing corresponding to critical values of the gain around which the recurrence process considerably slows down, switching between dynamical orbits of different kind. We present evidence for such phenomenon in a fiber optics experiment where the gain is finely tuned by means of Raman amplification. A theoretical explanation is also provided that matches almost perfectly with our experimental results.

DOI: 10.1103/PhysRevResearch.6.033335

I. INTRODUCTION

Modulational or Benjamin-Feir instability (MI) [1–3] is, in its most general meaning, the exponential amplification of a small perturbation at the expense of a strong background (pump) wave. It is a ubiquitous phenomenon in weakly nonlinear physical systems occurring in optics (both guided [2] and free space [4]), hydrodynamics of surface gravity waves [5], Langmuir waves in plasmas [6], and Bose-Einstein condensates [7]. In past decade much attention has been devoted to the fully nonlinear stage of MI past the initial amplification. Different scenarios are possible, which range from the formation of breather pairs [8] or the onset self-modulated structures for localized perturbations [9–11] to the recurrence (cycles of conversion and back-conversion between the perturbation and the background) characteristic of purely periodic perturbations, e.g., the typical case of a single injected sideband pair. The observation of the latter regime, pioneered in hydrodynamics [5] and investigated recently in more depth in optical fibers [12,13] and in bulk crystals [14], is particularly intriguing, not only because it is evocative of the famous Fermi-Pasta-Ulam-Tsingou phenomenon [15], but also because the recurrences are well organized according to a nontrivial phase-space structure ruled by the underlying simplest and universal model, namely, the nonlinear Schrödinger equation (NLSE) [16,17].

A full understanding of the nonlinear stage of MI is significant because MI is the underlying mechanism of extreme event (rogue wave) formation [18], as well as the generating mechanism behind frequency comb formation in damped-driven resonator systems [19], whose quasiconservative regime presents extremely complex evolution scenarios that remain to be explored experimentally [20]. In this sense, the integrable nature of the NLSE is appealing because it allows for a detailed description of the phase space associated with MI [21–23], whose main trait is the coexistence of two distinct types of recurrences [referred to below as shifted and unshifted, or period 2 (P2) and period 1 (P1), respectively], which can be selectively accessed by acting on the launching conditions. In particular, the dynamics of nonlinear MI in optical fibers was shown to be in excellent agreement with the NLSE solutions not only in early demonstrations based on cutback experiments [12,24–26], but also in more advanced results obtained through nondestructive reconstruction of the Fourier mode evolutions in amplitude and phase, performed via heterodyne detection of backscattered light [13,25,27–31].

One of the strongest conditions to observe the exact and rich regular dynamics associated with the NLSE over several recurrence periods, besides the low background noise [32], is the conservation of the total field intensity, which is achieved in the recent advanced experiments through counterpropagating Raman amplification. Albeit small, the natural energy dissipation in any propagation medium irreversibly spoils the possibility to observe long-term recurrences of P1 type, as reported in hydrodynamics [33]. In this respect, optical fibers turned out to be the ideal platform to detect the separatrix-crossing phenomenon from P1 to P2 orbits induced by dissipation [34]. The careful control of net losses through undercompensated Raman amplification enabled proof of multiple separatrix-crossing events occurring at critical values of the loss coefficient.

The goal of this paper is to investigate the analogous phenomenon in the presence of a net gain instead of dissipation. Indeed, in hydrodynamics, forcing naturally occurs from the action of the wind, and this was shown to yield the opposite effect, i.e., crossing from P2 to P1 [35,36]. However, an experimental demonstration of the phenomenon can be

*Contact author: andrea.armaroli@unife.it
†Contact author: arnaud.mussot@univ-lille.fr

Published by the American Physical Society under the terms of the Creative Commons Attribution 4.0 International license. Further distribution of this work must maintain attribution to the author(s) and the published article's title, journal citation, and DOI.

foreseen with much better precision in optics, where an unprecedented level of control of the forcing can be obtained by tuning the Raman pump to achieve slight overcompensation of the losses. This is the focus of the present work, where we present evidence of separatrix crossing induced by the weak linear amplification in optical fibers. On the one hand, the observation of the phenomenon allows us to understand whether such a crossing persists even when a major impact of noise amplification due to spontaneous MI must be expected in the presence of gain. On the other hand, this offers the possibility to tame the recurrence phenomenon by exploiting the dramatic slowing down of the dynamics, which is found to occur around the critical values of gain responsible for the crossing.

We first recall the theoretical approach of Ref. [34], based on two different perturbation approaches, and adapt it to gain; then we present the physical mechanism for gain tuning and recall the experimental setup. Compared with the case of dissipation, a different trade-off in fiber parameters is required to limit spurious noise amplification. We then report on the experimental results and their comparison to the theoretical and numerical predictions.

II. THEORY OF SEPARATRIX CROSSING FROM FORCING

Let us consider a generalized nonlinear Schrödinger equation (NLSE) including forcing [17]

$$i\frac{\partial E}{\partial Z} - \frac{\beta_2}{2}\frac{\partial^2 E}{\partial T^2} + \gamma|E|^2E = i\frac{g}{2}E, \tag{1}$$

where β_2 (ps^2/km) denotes the group-velocity dispersion, γ (W^{-1} km^{-1}) the nonlinear coefficient, g the linear gain (km^{-1}), and E (W$^{1/2}$) the complex envelope of the electric field propagating in the fiber; Z (km) and T (ps) are the propagation distance and time in the frame moving at the group velocity, respectively. In the focusing regime ($\beta_2\gamma < 0$), the T-independent solution of Eq. (1) $E = \sqrt{P_p}\exp(iP_pZ)$ is modulationally unstable.

It is convenient to cast Eq. (1) in dimensionless form by defining $t = T/T_0$; $z = Z/L_{\rm nl}$; $\psi = E/\sqrt{P_{\rm tot}}$, with $P_{\rm tot} \neq P_p$ the total power injected in the fiber, possibly including additional sideband contributions (discussed below); $L_{\rm nl} \equiv (\gamma P_{\rm tot})^{-1}$; and $T_0 \equiv \sqrt{L_{\rm nl}|\beta_2|}$. Finally, defining $\tilde{g} \equiv gL_{\rm nl}$, we write

$$i\frac{\partial\psi}{\partial z} + \frac{1}{2}\frac{\partial^2\psi}{\partial t^2} + |\psi|^2\psi = i\frac{\tilde{g}}{2}\psi. \tag{2}$$

A simple, yet qualitatively meaningful, analytical approach can be based on a mode truncation method (see Ref. [37] for a different context), which in the present case amounts to considering three-wave mixing (3WM), i.e., a pump and signal-idler sideband pair, as first discussed in Refs. [22,23] for $\tilde{g} = 0$ and used in [34] to analyze the effect of damping on separatrix crossing. We succinctly adapt it to the NLSE with amplification [Eq. (2)]. We recall that, for $\tilde{g} = 0$, by introducing the dimensionless angular frequency $\Omega = 2\pi f_m T_0$ related to the real-world modulation frequency f_m, MI occurs for $|\Omega| \leqslant 2$. In the simplest case of a single unstable mode $1 < \Omega \leqslant 2$, we can consider a perturbing pair of symmetric sidebands, also referred to as a signal-idler pair in the following. We define the ansatz

$$\psi(z,t) = \left(a_0(z) + \frac{a_1(z)}{\sqrt{2}}(e^{i\Omega t} + e^{-i\Omega t})\right)e^{(\tilde{g}/2)z} \tag{3}$$

and insert it in Eq. (2). The variables $a_{0,1}$ represent the complex amplitudes of the carrier and sidebands, respectively. By construction, they satisfy $|a_0|^2 + |a_1|^2 = 1$.

By neglecting all terms oscillating at $\pm m\Omega$, with $m \geqslant 2$, it is easy to verify that the dynamics takes place in a phase space defined by two effective canonical conjugate variables $\Delta\Phi = \arg(a_1) - \arg(a_0)$ and $\eta = |a_1|^2$. The evolution is conveniently expressed in terms of the rescaled distance $\bar{z} \equiv \frac{\exp(\tilde{g}z)-1}{\tilde{g}}$ as

$$\frac{d\eta}{d\bar{z}} = \frac{\partial H}{\partial\Delta\Phi}, \quad \frac{d\Delta\Phi}{d\bar{z}} = -\frac{\partial H}{\partial\eta},$$
$$H = \eta(1-\eta)\cos 2\Delta\Phi + \left(1 - \frac{\Omega^2}{2(1+\tilde{g}\bar{z})}\right)\eta - \frac{3}{4}\eta^2. \tag{4}$$

If $g = 0$, Eq. (4) describes a one-degree-of-freedom integrable Hamiltonian system, with H a constant of motion. (Note that, in the context of MI, a different Hamiltonian approach is possible, such as that in Ref. [38].) As discussed in detail in [22,23], the system evolves like a point mass in a double-well potential [see Fig. 1(a)]. Two distinct types of closed orbits (recurrences) are observed, depending on the initial conditions. They are illustrated in Figs. 1(b) and 1(d) using dimensional units in order to facilitate the comparison with the experiment. We use the parameters $\beta_2 = -21$ ps^2 km^{-1}, $\gamma = 1.3$ W^{-1} km^{-1}, $P_p(z=0) = 500$ mW, $P_s(z=0) = P_i(z=0) = 5$ mW, and $f_m = 39.6$ GHz, corresponding to the maximum of MI gain. For an initial condition with $H > 0$, the orbit resembles a figure eight and corresponds to successive peak conversions which are shifted by half a temporal period or $\Delta\Phi = \pi$ [Fig. 1(b)], whereas $H < 0$ yields a single-well type of orbits with conversion peaks always occurring in phase [Fig. 1(d)]. We refer to the former type of orbits as shifted or P2 and the latter as unshifted or P1. They are also referred to as type A or type B with reference to exact doubly periodic solutions of the NLSE [31]. The limit case $H = 0$ corresponds to the separatrix, where the orbit decays asymptotically to the background after a single growth stage as shown in Fig. 1(c). In turn this trajectory stands for a portion of the full Akhmediev breather (AB) that connects the background to itself at $z = \pm\infty$ [21]. For sufficiently weak input modulation $\eta(0) \ll 1$, this orbit requires a precise (frequency-dependent) input phase $\Delta\Phi_{\rm AB} = \frac{1}{2}\cos^{-1}(\Omega^2/2 - 1)$ [13]. We also emphasize that, though Eq. (4) provides only a qualitatively accurate description of the NLSE dynamics, the phase-space representation remains a very powerful tool, suitably valid for projecting exact multifrequency solutions of the NLSE too [31].

Obviously, when $\tilde{g} = 0$, the conservation of H constrains the system to stay on the orbit dictated by the initial condition, thus preventing the possibility of one type of orbit crossing into the other (different) type. Such a possibility, however, becomes allowed for $\tilde{g} \neq 0$. This was experimentally demonstrated by studying the influence of damping ($\tilde{g} < 0$) in fiber optics [34] and water waves [33] or forcing ($\tilde{g} > 0$) in water waves [36]. The former exhibits a transition from

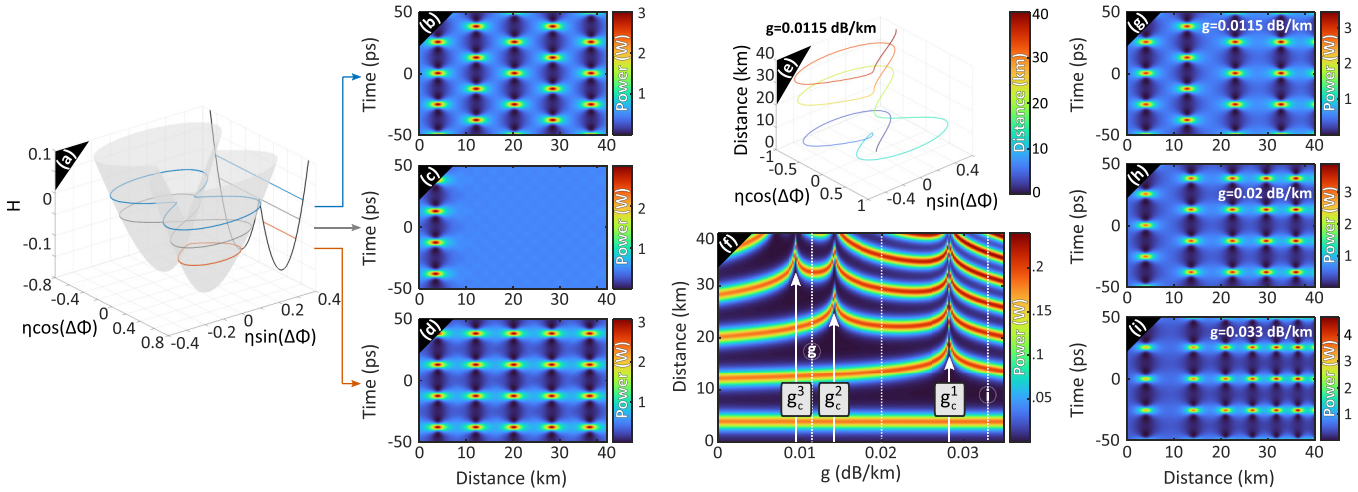

FIG. 1. (a) Hamiltonian surface $H = H(x, y)$ of integrable 3WM in the phase space $(x, y) \equiv (\eta\cos(\Delta\Phi), \eta\sin(\Delta\Phi))$ and its projection on the plane $\Delta\Phi = 0$ (black line in the vertical plane behind the H surface), with highlighted level curves corresponding to P2 ($H = -0.05$, orange line) and P1 ($H = 0.05$, blue line) orbits around the separatrix (AB, $H = 0$, gray line) and (b)–(d) corresponding space-time power evolutions from the conservative NLSE ($g = 0$). (e) Phase-space trajectory vs distance Z showing the separatrix crossing for $g = 0.0115$ dB/km. (f) False color plot of the signal power P_s evolutions along the fiber distance as a function of weak forcing g for the initial condition $\Delta\Phi(z = 0) = -\frac{\pi}{2}$ initially exciting a P2 orbit. (g)–(i) Examples of space-time power evolutions for $g = \{0.0115, 0.02, 0.033\}$ dB/km, corresponding to dashed vertical lines in (f). The parameters are $\beta_2 = -21$ ps^2 km^{-1}, $\gamma = 1.3$ W^{-1} km^{-1}, $P_p(z = 0) = 500$ mW, $P_s(z = 0) = P_i(z = 0) = 5$ mW, and $f_m = 39.6$ GHz.

P1 to P2 orbits, and vice versa (P2 to P1) in the latter. Here we present a detailed analysis of the impact of forcing in fiber optics. An illustration of this phenomenon is provided in Fig. 1(e), where the phase space is stroboscopically expanded in the propagation direction (vertical axis). It is apparent that a trajectory starting from a small $\eta(0) = \eta_0 \ll 1$ and $\Delta\Phi(0) = \Delta\Phi_0 = \pm\frac{\pi}{2}$ drops, after two phase-shifted recurrence cycles, onto an unshifted orbit.

A convenient way to illustrate the overall impact of forcing is to plot the evolution of the signal wave power $P_S = \frac{\eta P_{\rm tot}}{2}$ against distance as a function of g. In Fig. 1(f) we show the incidence of the linear amplification on an initially shifted excitation [$\Delta\Phi(z = 0) = -\frac{\pi}{2}$]. It is immediately clear that there exist some critical gain values g_c^n, $n = 1, 2, 3, \ldots$, ordered so that $g_c^1 > g_c^2 > g_c^3 > \cdots$, at which point the recurrence process slows down dramatically and yields anomalously large, yet finite (as verified numerically), recurrence distances. Such critical points originate from the separatrix crossing during the propagation and delimit transitions from shifted to unshifted recurrences. From the space-time power profiles in Figs. 1(g)–1(i) we deduce a general behavior according to the value of the gain. If $g_c^n < g < g_c^{n-1}$, the first n maximum compression points are consecutively shifted by half a temporal period while the successive ones are in-phase with the nth one. The separatrix crossing occurs then before—and very close to—the end of the nth passage close to the origin. We recall that, in the case of forcing, the system is not integrable anymore and the recurrence distance is not uniform and can deviate substantially from the doubly periodic solutions of the NLSE [31,39].

To describe such complex dynamics and predict the appearance of the critical gain values for separatrix crossing, we can rely on Eq. (4), similarly to Ref. [34]. The critical gain values $\tilde{g}_c^n$ for crossing are estimated as the solutions of

$$H_0 = -\frac{\tilde{g}_c^n \Omega^2}{2} \int_0^{nz_{\rm per}} e^{-\tilde{g}_c^n z} \eta(z) dz, \tag{5}$$

where $H_0 = \eta_0(1 - \eta_0)\cos(2\Delta\Phi_0) + (1 - \frac{\Omega^2}{2})\eta_0 - \frac{3}{4}\eta_0^2$ is the initial 3WM Hamiltonian, $z_{\rm per}$ is the longitudinal period without forcing, and $\eta(z)$ is the modulation power fraction along the orbit (see the Appendix). Indeed, Eq. (5) entails that the transition between the P2 and the P1 orbit that occurs when the Hamiltonian crosses the value $H = 0$ happens to take place at the nth back-conversion to the pump, which in turn corresponds to the nth passage near the origin [34]. This is justified heuristically by noting that under perturbed conditions it is only close to the origin of phase space that the two types of near-separatrix orbits can be clearly distinguished. A similar argument is used to characterize with the asymptotic method the separatrix crossing in one-dimensional oscillators with a double-well potential [40].

The $\tilde{g}_c^n$ values obtained from this Hamiltonian approach of the 3WM model are plotted as a function of the initial relative phase $\Delta\Phi_0$ and the signal to pump ratio $\frac{P_s}{P_p} = \frac{\eta_0}{2(1-\eta_0)}$ for $n = \{1, 2, 3\}$ in Fig. 2 (blue dashed lines). The critical gain g_c^n as a function of $\Delta\Phi_0$, as shown in Figs. 2(a), 2(c), and 2(e), exhibits a cosinelike shape (symmetric for $\Delta\Phi_0 \to -\Delta\Phi_0$). There exists a critical value of phase, which obviously corresponds to the separatrix phase $\Delta\Phi_{\rm AB}$, at which $g_c^n = 0$. For phase values in $[0; \Delta\Phi_{\rm AB}]$ and $[\pi - \Delta\Phi_{\rm AB}; \pi]$, $g_c^n < 0$ (damping), as the separatrix crossing occurs from P1 to P2 orbits, as in Ref. [34]. For values in $[\Delta\Phi_{\rm AB}; \pi - \Delta\Phi_{\rm AB}]$, $g_c^n > 0$, i.e., the case we are interested in here (Fig. 1). The critical gain values decrease in magnitude as $\Delta\Phi_{\rm AB}$ is approached.

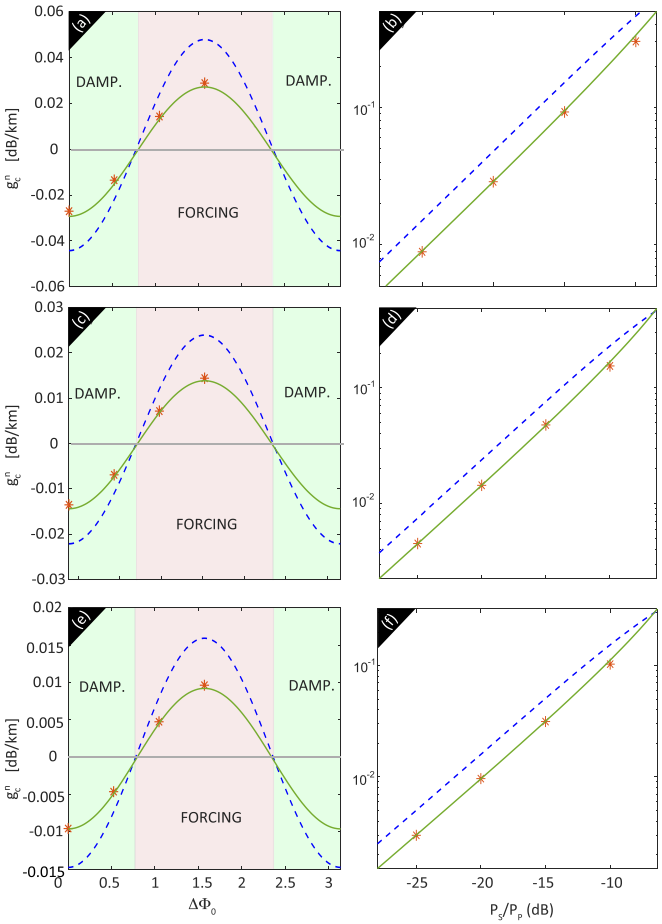

FIG. 2. Comparison of critical gain g_c^n as obtained from the 3WM model (5) (blue dashed line), the finite-gap approach (6) (green solid line), and NLSE simulations (crosses) vs (a), (c), and (e) the relative phase $\Delta\Phi_0$ for fixed $\eta_0 = 0.0196$ or vs sideband to pump power ratio η_0 for fixed $\Delta\Phi(0) = \frac{\pi}{2}$. The results are relative to first three crossing: (a) and (b) $n = 1$, (c) and (d) $n = 2$, and (e) and (f) $n = 3$. The other parameters are the same as in Fig. 1.

Noteworthily, the comparison of 3WM results (blue dashed line) and integration of Eq. 1 (red crosses) shows a considerable discrepancy, which is mainly due to the intrinsic error in the value of the spatial period $z_{\rm per}$ [see Eq. (A3) in the Appendix] compared with the corresponding NLSE estimate. A substantially more accurate approach is found in [41], based on the perturbation theory of finite-gap integration of the NLSE (see also [42] for the unperturbed case). We remark that such an approach is limited to integrable systems such as the NLSE, at variance with the 3WM approach that can be easily extended to models which lack integrability, yet present an underlying homoclinic structure of recurrent MI (see, e.g., [43,44]). From the finite-gap approach, which is valid for small input modulation amplitudes and weak amplification ($\tilde{g} \ll 1$), a simple formula can be derived for the critical gain values $\tilde{g} = \tilde{g}_c^n$ (for details we refer the reader to [34,41]),

$$\tilde{g}_c^n = \frac{\eta_0(1-\eta_0)e_+e_-}{2ng_{\rm MI}}, \tag{6}$$

where η_0 is the modulation power fraction; $e_\pm \equiv \frac{1}{\sqrt{2}}(e^{i\mp\psi}e^{-i\Delta\Phi_0} - e^{i\pm\psi}e^{i\Delta\Phi_0})$, with $\psi \equiv \cos^{-1}\frac{\Omega}{2\sqrt{1-\eta_0}}$, are the growing and decaying eigenvectors of MI, as defined in [41,42]; and $g_{\rm MI} = \frac{\Omega}{2}\sqrt{4(1-\eta_0)-\Omega^2}$ is the normalized MI gain. We notice in Figs. 2(a), 2(c), and 2(e) that this analytical estimate (green solid lines) follows the same cosine trend in $\Delta\Phi(z=0)$ as for the 3WM model, but with an error below 5%, compared to nearly a factor of 2 overestimate for the 3WM at $\Delta\Phi_0 = \frac{\pi}{2}$.

It is also interesting to consider how g_c^n depends on $\frac{P_S}{P_P}$ (or equivalently η_0). We show the numerical as well as the analytical results in Figs. 2(b), 2(d), and 2(f) for $n = 1, 2, 3$. The critical value grows exponentially with the signal power fraction. Both analytical estimates are qualitatively satisfactory. While Eq. (5) always grossly overestimates g_c^n, Eq. (6) is almost indistinguishable from numerical results at small $\frac{P_S}{P_P} < -15$ dB, while it slightly overestimates g_c^n at larger ratios, though the low error (less than 15%) allows us to conclude that finite-gap theory perform well even beyond its expected limit of validity, i.e., extremely weak sidebands.

After having assessed the validity and limits of our analytical estimates, we describe the experimental setup and compare numerical and analytical results to experimental recordings.

III. EXPERIMENT

A. Experimental setup

To experimentally study separatrix crossing in the nonlinear stage of MI induced by a weak forcing, the key feature is the careful control of the net gain experienced by the signal during the propagation in the fiber. To this end, we use the backward Raman pumping scheme. While in [13,27,28,30–32] the same scheme was used to achieve nearly optimal cancellation of the losses, thus enabling almost fully transparent propagation, here the Raman pump power is tuned above this optimum to get a net effective gain. To calibrate the effective gain value associated with a specific Raman pump power value, we have recorded, for different multiple values of the Raman pump power, the optical time domain reflectometer (OTDR) traces obtained from the propagation of pulses. We use weak pulses to make the nonlinear effects negligible in the calibration. Indeed, pulse powers below 50 mW result in nonlinear lengths longer than 17 km, which exceed the typical fiber span.

Two examples of OTDR traces are plotted in Figs. 3(a) and 3(b) for injected Raman pump powers of $P_{\rm R}(z=L) = 200$ and 410 mW, respectively (these values are the Raman pump range limits). In order to evaluate the net effective gain $g_{\rm eff}$, we fit the observed traces by exponential curves, i.e., $\exp(g_{\rm eff}Z)$, displayed as dashed lines in Figs. 3(a) and 3(b). We find that Raman pump power below $P_{\rm R}^{\rm opt} = 240$ mW results in net losses [negative slope exponential, i.e., negative gain; see Fig. 3(a)], whereas above this value the exponential fit gives a net gain, as shown by yellow dashed line in Fig. 3(b). The results of this procedure for different values of $P_{\rm R}$ are summarized in Fig. 3(c). In the following observations of the separatrix crossing, we use the linear fit in Fig. 3(c) to assess the resulting net gain $g_{\rm eff}$ corresponding to the value of $P_{\rm R}$ actually employed in nonlinear experiments.

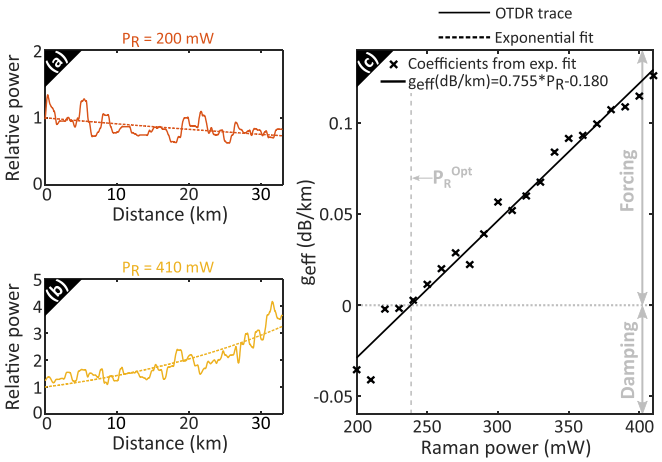

FIG. 3. Relative evolutions of the backscattered signal power with (a) $P_R(z = L) = 200$ mW (orange solid line) and (b) $P_R(z = L) = 410$ mW (yellow solid line). The corresponding dashed lines stand for the exponential fit. (c) Net effective gain as a function of the Raman pump power P_R.

To demonstrate the influence of forcing on the nonlinear MI recurrences, we use a fully fiber optic setup based on multiheterodyning reflectometry, quite similar to the one used in [13,27,28,30–32] and particularly to [34], though with some important differences that we detail in the following. Since we overcompensate for the losses, spontaneous MI amplification of noise may lead to thermalization [32]. In order to prevent such a detrimental effect, we use an SMF-28 fiber span of 16.73 km (shorter compared to the span of approximately 20 km used in [34]) and increase the pump power to reduce the nonlinear length as well. This allows us to achieve both a sufficient number of recurrence cycles (at least 3 to be able to also observe the transition around g_c^2) within the fiber span and a higher sideband-to-noise ratio. The signal to pump ratio is then set to $\frac{P_s(z=0)}{P_p(z=0)} = -9.5$ dB and the P_R maximum value to 410 mW, which allows us to get an effective gain g_{eff} up to 0.13 dB/km. The initial relative phase we usually set to excite a shifted orbit is $\Delta\Phi_0 = \pm\pi/2$ [13]. However, for such an input phase, we expect from numerical simulations that $g_c^1 = 0.268$ dB/km, which is beyond the achievable effective gain range. To get a smaller critical gain, we need to choose a $\Delta\Phi_0$ value closer to the separatrix so that it requires a weaker perturbation to cross it (as predicted by the 3WM model and the finite-gap theory; see Fig. 2). We set then the initial relative phase to $\Delta\Phi_0 = -0.28\pi$. From the input pump power $P_p(z = 0) = 470$ mW and the fiber parameters $\beta_2 = -21$ ps^2 km^{-1} and $\gamma = 1.3$ W^{-1} km^{-1}, we calculate the frequency of maximum MI gain at $f_{\text{peak}} = 38.4$ GHz. We set the modulation frequency very close to that value, at $f_m = 38.2$ GHz.

B. Experimental results

Here we discuss the experimental characterization of the recurrence phenomenon in the presence of linear gain. We display the evolution of the signal power $P_s(z)$ and the relative phase $\Delta\Phi(z)$ as a function of the effective gain in Figs. 4(a) and 4(b), respectively. Three different regions labeled 3, 2, and 1 (from left to right) are outlined. In region 3 the system is close to optimal compensation of losses, with either a slight attenuation (down to $g_{\text{eff}} = -0.029$ dB/km) or a slight amplification (up to $g_{\text{eff}} = g_{\text{eff},c}^2 = 0.043$ dB/km). Within the finite length of the fiber used in the experiment, in this region gain has only the minor effect of slightly changing the recurrence distance. Looking at the power evolution in Fig. 4(a), we observe three complete recurrences, but also a π shift between successive conversion cycles, as clearly shown by the phase evolution in Fig. 4(b). This behavior is confirmed by the reconstructed trajectory in the phase space in Fig. 4(c) obtained for a specific effective gain $g_{\text{eff}} = -0.021$ dB/km ($P_R = 210$ mW). The orbit oscillates from the right to the left (and vice versa) half phase space between two consecutive growth-decay cycles, meaning that two consecutive maximum compression points are shifted by half a temporal period. This dynamic is not surprising because it behaves exactly the same as a shifted orbit excitation in the integrable limit $g = 0$. These experimental results can be compared to the numerical results in Figs. 4(f)–4(j). These numerical data were obtained with a slightly different initial relative phase value than the experimental one. Indeed, the numerical results with $\Delta\Phi_0 = -0.28\pi$ do not predict any critical transition point for $g < 0.13$ dB/km. Thus, in our numerical simulations, we employ a slightly different value $\Delta\Phi_0 = -0.335\pi$. We suggest that such a discrepancy can simply be due to an imperfect control of the initial relative phase, which is set through a Waveshaper [13,29]. Indeed, while a small shift of the initial relative phase is not detrimental far from $\Delta\Phi_{\text{AB}}$, it can have a very strong impact on the dynamics close to it. When we account for such a difference in the initial phase, we find very good agreement between experiments and numerics in region 3 (as well as in regions 2 and 1 described below).

By increasing the effective gain up to $g_{\text{eff},c}^2 = 0.043$ dB/km ($P_R = 295$ mW), we notice that the third recurrence cycle period increases so that the corresponding conversion peak does not appear within the fiber length close to $g_{\text{eff},c}^2$. Beyond this critical gain point, in region 2, we record three conversion peaks again. However, the phase evolution reveals that there is no longer a π phase shift between the second and third recurrence cycles. This is confirmed by the phase-space representation in Fig. 4(d) with $g_{\text{eff}} = 0.062$ dB/km ($P_R = 320$ mW). While the trajectory initially spans the full phase space, as expected for a P2 orbit, the third recurrence of power fraction η occurs in the left half plane, i.e., the trajectory has switched to a P1 orbit: The separatrix has been crossed between the second and third recurrence cycles.

When approaching $g_{\text{eff},c}^1 = 0.088$ dB/km ($P_R = 355$ mW), the period of the second cycle also increases and the corresponding conversion peak spatially shifts at a higher distance. However, beyond $g_{\text{eff},c}^1$, the trend inverts and the number of conversion peaks recorded within the fiber length increases up to 4 at $g_{\text{eff}} = 0.13$ dB/km in region 1. In this region, the phase remains bounded in $[-\frac{\pi}{2}; \frac{\pi}{2}]$, similarly to what has been observed in conservative systems for a P1 orbit excitation. This is further revealed by the trajectory in the phase space in Fig. 4(e) for $g_{\text{eff}} = 0.114$ dB/km, where all

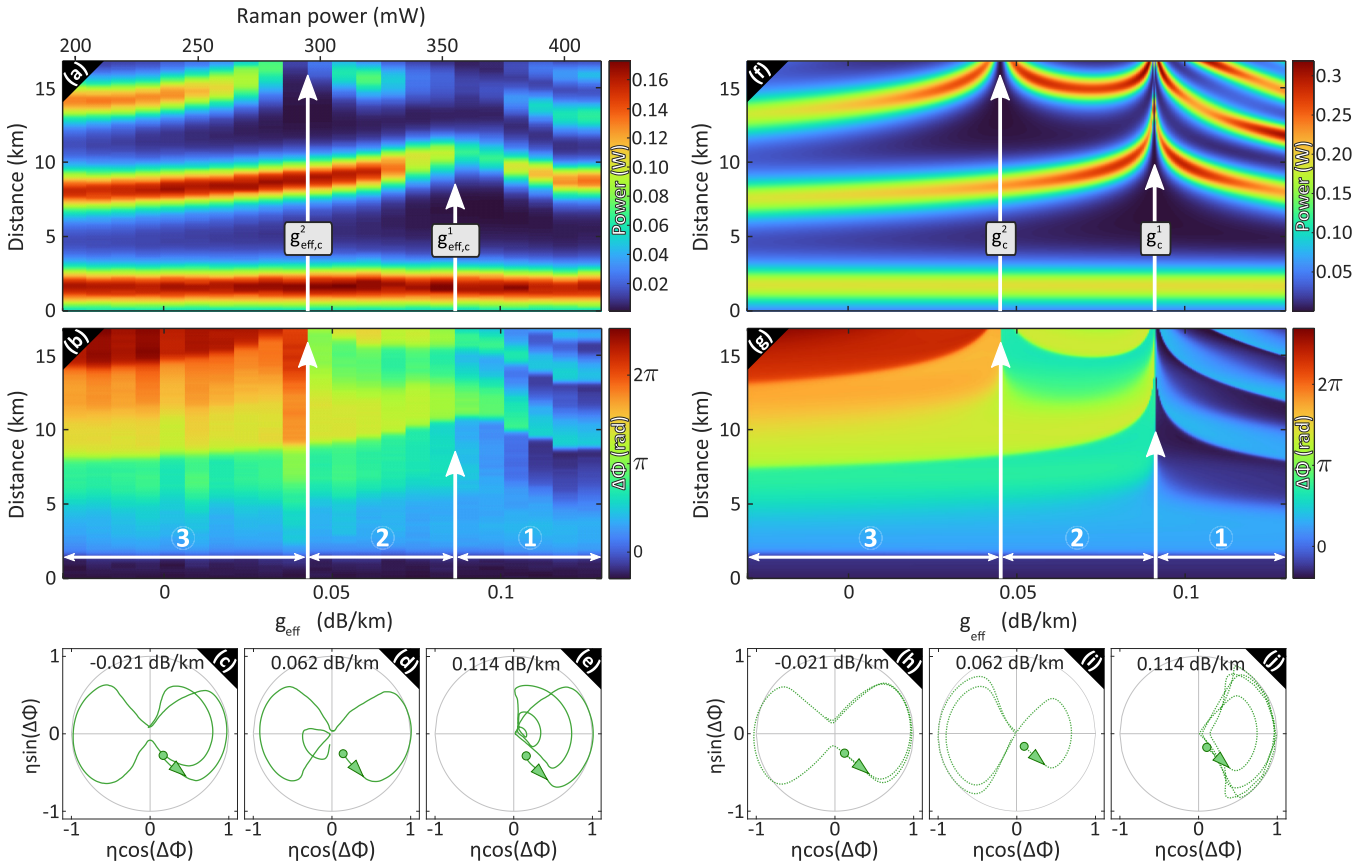

FIG. 4. False color plots of (a) and (f) the signal power evolution and (b) and (g) the relative phase along the fiber length as a function of the effective gain. (c)–(e) and (h)–(j) Trajectories in the phase space ($\eta\cos(\Delta\Phi)$, $\eta\sin(\Delta\Phi)$) for $g_{\rm eff} = -0.021$, 0.062, and 0.114 dB/km. (a)–(e) Experimental data and (f)–(j) numerical simulations from the forced NLSE (1).

the trajectory stays in the right half-plane; all four compression points occur in phase. In this case the separatrix has been crossed during the first growth and decay cycle, leading to an unshifted orbit excitation from the second one. The overall agreement between experiments and numerical simulations is good in regions 1 and 2, except for the fact that the recorded signal power exhibits much lower power levels compared with simulations during the third and fourth recurrences [compare Figs. 4(a) and 4(f)]. This can be attributed to the blurring effect from slight fluctuations of the parameters but especially to noise-induced MI. Indeed, we notice a decrease of the signal power maxima, similarly to what is observed in [32]. Regarding the critical gain values, we find $g^1_{{\rm eff},c} = 0.088$ dB/km ($P_{\rm R} = 355$ mW) and $g^2_{{\rm eff},c} = 0.043$ dB/km ($P_{\rm R} = 295$ mW), which follow almost perfectly the inverse scaling with n, predicted by Eq. (6), at variance with the case of damping induced crossing [34], which exhibited a significant discrepancy between the observed critical values of losses and their scaling with n. We conjecture that this could be due to the fact that here the system is initially excited close to A-type or P2 solutions of the NLSE, which are known to be more stable and robust to the input three-wave truncation due to their intrinsic Fourier structure [31,39]. Finally, from the numerical data shown in Figs. 4(f) and 4(g), we obtain good agreement; the extrapolated numerical values are $g^1_c = 0.091$ dB/km and $g^2_c = 0.045$ dB/km, though obtained for $\Delta\Phi(z = 0) = -0.335\pi$.

Finally, we emphasize that weaker amplifications result in critical values of gain which become more densely spaced. However, as clear from the trend in Fig. 1(f), the weaker the critical gain, the longer the distance required to observe it. Therefore, in the present experiment performed at fixed fiber length, we are limited to the first two critical values of gain, since the use of longer fibers would require us to improve the present Raman amplification based control of gain, an issue which is left for future work.

IV. CONCLUSION

Due to an accurate control, via counterpropagating Raman amplification, of the linear gain experienced by light during propagation in an optical fiber, we probed the behavior of Fermi-Pasta-Ulam-Tsingou–like recurrences in the nonlinear stage of MI. We showed that forcing leads the shifted orbits of recurrent MI to be converted into unshifted ones. We found critical values of linear gain at which separatrix crossing occurs almost precisely after n recurrence cycles: In the fiber span considered, we were able to distinguish three regions separated by the lowest-order values of g^n_c, with $n = 1, 2$. In order to observe higher-order critical values of gain, we would need a longer fiber span and a more accurate gain profile shaping, i.e., a more sophisticated control of the Raman pump. Apart from the interest in taming and controlling nonlinear effects in an optical fiber, we expect to spur a fundamental

interest in the behavior of other physical systems such as those with quadratic nonlinear response [45] or pendulum chains [46] that exhibit similar homoclinic-heteroclinic connection in MI.

ACKNOWLEDGMENTS

This research was supported by IRCICA (USR 3380 CNRS), Agence Nationale de la Recherche (Programme Investissements d'Avenir, FARCO) Ministry of Higher Education and Research; Hauts de France Council; and European Regional Development Fund (Photonics for Society P4S, WAVETECH, FELANI, GPEG). A.A. and S.T. acknowledge funding from the Ministry of University and Research of Italy (Grants No. PRIN2020X4T57A and No. PRIN2022NCTCY, NextGenerationEU, with the European Union).

APPENDIX: THE 3WM APPROXIMATION AND EQ. (5)

When $\tilde{g} \neq 0$, the Hamiltonian of the 3WM system [Eq. (4)] is no longer conserved but rather increases according to the equation (we refer the reader to Ref. [34] for its derivation)

$$\frac{dH}{dz} = \frac{\tilde{g}}{2}\Omega^2 e^{-\tilde{g}z}\eta(z). \tag{A1}$$

Integration of such an equation between $z = 0$ and $z = nz_{\rm per}$, i.e., n periods of the power exchange of P2 orbits, leads to Eq. (5), provided we set $H_0 = H(z = 0)$ and consider that crossover into unshifted (P1) orbits occurs at the characteristic value $H = H(nz_{\rm per}) = H_{\rm saddle} = 0$.

While Eq. (A1) involves only the approximation related to mode truncation, in Eq. (5) we necessarily approximate the sidebands power fraction $\eta(z)$ with its unperturbed ($\tilde{g} = 0$) value [22], as

$$\eta(z) = \frac{a_-(b_+ - b_-)\mathrm{sn}^2(\rho(z - z_0)|m) - b_-(b_+ - a_-)}{(b_+ - b_-)\mathrm{sn}^2(\rho(z - z_0)|m) - (b_+ - a_-)}, \tag{A2}$$

where $\rho = \sqrt{7(a_+ - b_-)(b_+ - a_-)}/4$, $m = \frac{(b_+ - b_-)(a_+ - a_-)}{(a_+ - b_-)(b_+ - a_-)}$ is the modulus of the Jacobian sn function, z_0 is a suitable constant, and $a_+ \geqslant b_+ \geqslant b_- \geqslant a_-$ read $\{a_+, b_-\} = \Omega^2 \pm \sqrt{\Omega^4 + 4H_0}$ and $\{b_+, a_-\} = \frac{2}{7}[2 - \Omega^2/2 \pm \sqrt{(2 - \Omega^2/2)^2 - 7H_0}]$. The spatial period $z_{\rm per}$ of the solution (A2) can be expressed in terms of the elliptic integral of the first kind $K(m)$ as

$$z_{\rm per} = \frac{2K(m)}{\rho} \simeq \frac{1}{\rho}\log\frac{4}{\sqrt{1 - m}}, \tag{A3}$$

where the logarithmic approximation is valid for $m \simeq 1$, i.e., near the separatrix. We emphasize that $z_{\rm per}$ is the period of power evolution while the spatial period of the figure-of-eight orbit in the phase plane [see Figs. 1(a) and 1(b)] is $2z_{\rm per}$. In other words, $\eta(z)$ takes back its initial value twice along this type of orbit, while the relative phase $\Delta\Phi$ exhibits π increments.

We emphasize that Eq. (5) gives an excellent estimate of the critical values of gain for crossing which can be found from numerical integration of 3WM equations. However, as the full NLSE is concerned, the discrepancy discussed in Fig. 2 with the better estimate from finite-gap approach [Eq. (6)] essentially arises from the deviation of the period estimated from Eq. (A3) with respect to that of the full wave dynamics, reported in [39].

[1] T. B. Benjamin and J. E. Feir, The disintegration of wave trains on deep water Part 1. Theory, J. Fluid Mech. **27**, 417 (1967).
[2] K. Tai, A. Hasegawa, and A. Tomita, Observation of modulational instability in optical fibers, Phys. Rev. Lett. **56**, 135 (1986).
[3] V. Zakharov and L. Ostrovsky, Modulation instability: The beginning, Physica D **238**, 540 (2009).
[4] R. A. Fuerst, D.-M. Baboiu, B. Lawrence, W. E. Torruellas, G. I. Stegeman, S. Trillo, and S. Wabnitz, Spatial modulational instability and multisolitonlike generation in a quadratically nonlinear optical medium, Phys. Rev. Lett. **78**, 2756 (1997).
[5] B. M. Lake, H. C. Yuen, H. Rungaldier, and W. E. Ferguson, Nonlinear deep-water waves: Theory and experiment. Part 2. Evolution of a continuous wave train, J. Fluid Mech. **83**, 49 (1977).
[6] S. Thornhill and D. ter Haar, Langmuir turbulence and modulational instability, Phys. Rep. **43**, 43 (1978).
[7] J. H. V. Nguyen, D. Luo, and R. G. Hulet, Formation of matter-wave soliton trains by modulational instability, Science **356**, 422 (2017).
[8] B. Kibler, A. Chabchoub, A. Gelash, N. Akhmediev, and V. E. Zakharov, Superregular breathers in optics and hydrodynamics: Omnipresent modulation instability beyond simple periodicity, Phys. Rev. X **5**, 041026 (2015).
[9] G. Biondini and D. Mantzavinos, Universal nature of the nonlinear stage of modulational instability, Phys. Rev. Lett. **116**, 043902 (2016).
[10] M. Conforti, S. Li, G. Biondini, and S. Trillo, Auto-modulation versus breathers in the nonlinear stage of modulational instability, Opt. Lett. **43**, 5291 (2018).
[11] A. E. Kraych, P. Suret, G. El, and S. Randoux, Nonlinear evolution of the locally induced modulational instability in fiber optics, Phys. Rev. Lett. **122**, 054101 (2019).
[12] G. Van Simaeys, P. Emplit, and M. Haelterman, Experimental demonstration of the Fermi-Pasta-Ulam recurrence in a modulationally unstable optical wave, Phys. Rev. Lett. **87**, 033902 (2001).
[13] A. Mussot, C. Naveau, M. Conforti, A. Kudlinski, F. Copie, P. Szriftgiser, and S. Trillo, Fibre multi-wave mixing combs reveal the broken symmetry of Fermi–Pasta–Ulam recurrence, Nat. Photon. **12**, 303 (2018).
[14] D. Pierangeli, M. Flammini, L. Zhang, G. Marcucci, A. J. Agranat, P. G. Grinevich, P. M. Santini, C. Conti, and E. DelRe, Observation of Fermi-Pasta-Ulam-Tsingou recurrence and its exact dynamics, Phys. Rev. X **8**, 041017 (2018).
[15] E. Fermi, J. R. Pasta, and S. Ulam, Studies of nonlinear problems, Los Alamos National Laboratory Report No. LA-1940, 1955 (unpublished).

[16] M. J. Ablowitz, B. Prinari, and A. D. Trubatch, *Discrete and Continuous Nonlinear Schrödinger Systems*, 1st ed. (Cambridge University Press, Cambridge, 2003).
[17] G. Agrawal, *Nonlinear Fiber Optics* (Academic, New York, 2012).
[18] J. M. Dudley, G. Genty, A. Mussot, A. Chabchoub, and F. Dias, Rogue waves and analogies in optics and oceanography, Nat. Rev. Phys. **1**, 675 (2019).
[19] T. Hansson, D. Modotto, and S. Wabnitz, Dynamics of the modulational instability in microresonator frequency combs, Phys. Rev. A **88**, 023819 (2013).
[20] F. Coppini and P. M. Santini, Fermi-Pasta-Ulam-Tsingou recurrence of periodic anomalous waves in the complex Ginzburg-Landau and in the Lugiato-Lefever equations, Phys. Rev. E **102**, 062207 (2020).
[21] N. N. Akhmediev and V. I. Korneev, Modulation instability and periodic solutions of the nonlinear Schrödinger equation, Theor. Math. Phys. **69**, 1089 (1986).
[22] G. Cappellini and S. Trillo, Third-order three-wave mixing in single-mode fibers: Exact solutions and spatial instability effects, J. Opt. Soc. Am. B **8**, 824 (1991).
[23] S. Trillo and S. Wabnitz, Dynamics of the nonlinear modulational instability in optical fibers, Opt. Lett. **16**, 986 (1991).
[24] K. Hammani, B. Wetzel, B. Kibler, J. Fatome, C. Finot, G. Millot, N. Akhmediev, and J. M. Dudley, Spectral dynamics of modulation instability described using Akhmediev breather theory, Opt. Lett. **36**, 2140 (2011).
[25] X. Hu, W. Chen, Y. Lu, Z. Yu, M. Chen, and Z. Meng, Distributed measurement of Fermi–Pasta–Ulam recurrence in optical fibers, IEEE Photonics Technol. Lett. **30**, 47 (2018).
[26] A. Bendahmane, A. Mussot, A. Kudlinski, P. Szriftgiser, M. Conforti, S. Wabnitz, and S. Trillo, Optimal frequency conversion in the nonlinear stage of modulation instability, Opt. Express **23**, 30861 (2015).
[27] C. Naveau, P. Szriftgiser, A. Kudlinski, M. Conforti, S. Trillo, and A. Mussot, Experimental characterization of recurrences and separatrix crossing in modulational instability, Opt. Lett. **44**, 5426 (2019).
[28] C. Naveau, P. Szriftgiser, A. Kudlinski, M. Conforti, S. Trillo, and A. Mussot, Full-field characterization of breather dynamics over the whole length of an optical fiber, Opt. Lett. **44**, 763 (2019).
[29] C. Naveau, G. Vanderhaegen, P. Szriftgiser, G. Martinelli, M. Droques, A. Kudlinski, M. Conforti, S. Trillo, N. Akhmediev, and A. Mussot, Heterodyne optical time domain reflectometer combined with active loss compensation: A practical tool for investigating Fermi Pasta Ulam recurrence process and breathers dynamics in optical fibers, Front. Phys. **9**, 637812 (2021).
[30] G. Vanderhaegen, P. Szriftgiser, A. Kudlinski, M. Conforti, S. Trillo, M. Droques, and A. Mussot, Observation of four Fermi-Pasta-Ulam-Tsingou recurrences in an ultra-low-loss optical fiber, Opt. Express **28**, 17773 (2020).
[31] G. Vanderhaegen, P. Szriftgiser, C. Naveau, A. Kudlinski, M. Conforti, S. Trillo, N. Akhmediev, and A. Mussot, Observation of doubly periodic solutions of the nonlinear Schrödinger equation in optical fibers, Opt. Lett. **45**, 3757 (2020).
[32] G. Vanderhaegen, P. Szriftgiser, A. Kudlinski, M. Conforti, A. Armaroli, and A. Mussot, Observation of the noise-driven thermalization of the Fermi-Pasta-Ulam-Tsingou recurrence in optical fibers, Phys. Rev. A **106**, 033519 (2022).
[33] O. Kimmoun, H. C. Hsu, H. Branger, M. S. Li, Y. Y. Chen, C. Kharif, M. Onorato, E. J. R. Kelleher, B. Kibler, N. Akhmediev, and A. Chabchoub, Modulation instability and phase-shifted Fermi-Pasta-Ulam recurrence, Sci. Rep. **6**, 28516 (2016).
[34] G. Vanderhaegen, P. Szriftgiser, A. Kudlinski, A. Armaroli, M. Conforti, A. Mussot, and S. Trillo, Experimental tweaking of symmetry breaking in recurrent nonlinear modulational instability, Phys. Rev. A **108**, 033507 (2023).
[35] A. Armaroli, D. Eeltink, M. Brunetti, and J. Kasparian, Nonlinear stage of Benjamin-Feir instability in forced/damped deep-water waves, Phys. Fluids **30**, 017102 (2018).
[36] D. Eeltink, A. Armaroli, C. Luneau, H. Branger, M. Brunetti, and J. Kasparian, Separatrix crossing and symmetry breaking in NLSE-like systems due to forcing and damping, Nonlinear Dyn. **102**, 2385 (2020).
[37] S. Raghavan, A. Smerzi, S. Fantoni, and S. R. Shenoy, Coherent oscillations between two weakly coupled Bose-Einstein condensates: Josephson effects, π oscillations, and macroscopic quantum self-trapping, Phys. Rev. A **59**, 620 (1999).
[38] Z. Rapti, P. G. Kevrekidis, A. Smerzi, and A. R. Bishop, Variational approach to the modulational instability, Phys. Rev. E **69**, 017601 (2004).
[39] M. Conforti, A. Mussot, A. Kudlinski, S. Trillo, and N. Akhmediev, Doubly periodic solutions of the focusing nonlinear Schrödinger equation: Recurrence, period doubling, and amplification outside the conventional modulation-instability band, Phys. Rev. A **101**, 023843 (2020).
[40] F. J. Bourland and R. Haberman, Separatrix crossing: Time-invariant potentials with dissipation, SIAM J. Appl. Math. **50**, 1716 (1990).
[41] F. Coppini, P. G. Grinevich, and P. M. Santini, Effect of a small loss or gain in the periodic nonlinear Schrödinger anomalous wave dynamics, Phys. Rev. E **101**, 032204 (2020).
[42] P. Grinevich and P. Santini, The exact rogue wave recurrence in the NLS periodic setting via matched asymptotic expansions, for 1 and 2 unstable modes, Phys. Lett. A **382**, 973 (2018).
[43] S. Trillo and S. Wabnitz, Nonlinear modulation of coupled waves in birefringent optical fibers, Phys. Lett. A **159**, 252 (1991).
[44] C. De Angelis, M. Santagiustina, and S. Trillo, Four-photon homoclinic instabilities in nonlinear highly birefringent media, Phys. Rev. A **51**, 774 (1995).
[45] S. Trillo and F. Baronio, From regular to pseudo-stochastic recurrence of modulation instability in cascaded second-harmonic generation, Opt. Lett. **48**, 1284 (2023).
[46] A. R. Bishop, D. McLaughlin, M. Forest, and E. A. Overman, Quasi-periodic route to chaos in a near-integrable PDE: Homoclinic crossings, Phys. Lett. A **127**, 335 (1988).